Silicon Carbide Micro-devices for Combustion Gas Sensing under Harsh Conditions

Semi-annual Technical Report
Reporting Period:
April 1, 2004 to September 30, 2004

Ruby N. Ghosh[1], Peter Tobias[1] and Roger G. Tobin[2]

October 2004

DOE Award Number: DE-FC26-03NT41847

[1]Center for Sensor Materials and Dept. of Physics & Astronomy
2167 Biomedical Physical Sciences Building
Michigan State University

[2]Dept. of Physics and Astronomy
4 Colby St.
Tufts University

ABSTRACT

A sensor based on the wide bandgap semiconductor, silicon carbide (SiC), has been developed for the detection of combustion products in power plant environments. The sensor is a catalytic gate field effect device that can detect hydrogen containing species in chemically reactive, high temperature environments. For these capacitive sensors we have determined that the optimum sensor operating point in terms of sensor lifetime and response time is at midgap. Detailed measurements of the oxide leakage current as a function of temperature were performed to investigate the high temperature reliability of the devices. In addition, robust metallization and electrical contacting techniques have been developed for device operation at elevated temperatures. To characterize the time response of the sensor responses in the millisecond range, a conceptually new apparatus has been built. Using laser induced fluorescence imaging techniques we have shown that that the gas underneath the sensor can be completely exchanged with a time constant under 1 millisecond. Ultrahigh vacuum studies of the surface chemistry of the platinum gate have shown that sensor deactivation by adsorbed sulfur is a possible problem. Investigations on the chemical removal of sulfur by catalytic oxidation or reduction are continuing.

TABLE OF CONTENTS

DISCLAIMER 2
ABSTRACT 2
LIST(S) OF GRAPHICAL MATERIALS 4
1. INTRODUCTION 5
2. EXECUTIVE SUMMARY 6
3. EXPERIMENTAL 8
3.1 Samples 8
3.1.1 Fabrication of new samples 9
3.1.2 Metal deposition 9
3.1.3 Contact to the metal gates 10
3.2 Time-resolved fast sensor test assembly 10
3.2.1 Motivation for characterizing the set-up with an independent method 10
3.2.2 Characterizing the set-up with laser induced fluorescence (LIF) 11
3.3 Sensor measurements at the National Laboratory in Morgantown 14
3.4 Leakage current measurements 15
3.5 UHV surface chemistry 17
3.5.1 Sample mounting and thermometry 18
3.5.2 Surface cleaning 18
3.5.3 Temperature programmed desorption 19
3.5.4 Techniques for studying sulfur contamination 21
3.5.5 Design and fabrication of sensor samples for UHV studies 21
4. RESULTS AND DISCUSSION 23
4.1 Characterizing of the set-up with Moving Gas Outlets (MGO) 23
4.2 High-temperature reliability studies 24
4.2.1 Optimum sensor operating point 24
4.2.2 Gate leakage current measurements at high temperature 24
4.3 UHV surface chemistry of the Pt gate 26
4.3.1 CO adsorption and temperature calibration 26
4.3.2 Sulfur contamination studies 27
5. CONCLUSION 31
ACKNOWLEDGEMENTS 31
REFERENCES 32
BIBLIOGRAPHY 33
LIST OF ACRONYMS AND ABBREVIATIONS 34

LIST(S) OF GRAPHICAL MATERIALS

Fig. 1.1 Schematic of a SiC field-effect sensor for H_2-containing gases 6
Fig. 3.1.1 Schematic cross section of the MISiC capacitor 8
Fig. 3.2.1. Photo of the moving gas outlets 11
Fig. 3.2.2a. Set-up for fast sensor measurements 12
Fig.3.2.2b. Laser induced fluorescence image of the moving gas outlets 13
Fig.3.2.2c. Laser induced fluorescence image 2.4 ms after the trigger pulse 14
Fig. 3.3. Set-up for sensor measurements in National Laboratory in Morgantown. 15
Table 3.4. Details of the samples used to investigate high temperature reliability 17
Fig. 3.5.2. Auger spectra of Pt gate, showing sample cleaning 19
Fig. 3.5.3a. Schematic diagram of the electrostatic shield for TPD 20
Fig. 3.5.3b. Pressure-time traces measured by the QMS, with and without bias 21
Fig. 3.5.5. Sample for UHV sensor response and surface chemistry studies. 22
Fig 4.1. Displacement of the moving gas outlets in time 23
Fig. 4.2.1. Band alignment of the interface between SiO_x, Si and SiC 24
Fig. 4.2.2a**.** Leakage current density vs. temperature for 6H-SiC n-type devices. 25
Fig. 4.2.2a**.** Leakage current density vs. temperature for 4H-SiC n-type devices. 26
Fig. 4.3.1. TPD spectrum (mass 28) after CO adsorption at 180 K. 27
Fig. 4.3.2a. Surface coverage of sulfur during various treatments in UHV 28
Fig. 4.3.2b. Surface coverage of sulfur during various treatments in UHV 29
Fig. 4.3.2c. SO_2 TPD traces after dosing with sulfur and oxygen 29
Fig. 4.3.2d . TPD spectra after O_2 exposure onto the clean Pt surface 30

1. INTRODUCTION

Emissions control for the energy sector requires gas sensors that can operate in chemically reactive high temperature environments for both real time monitoring and feedback control of exhaust products. Gaseous species that need to be monitored include hydrogen, hydrocarbons, nitrogen oxides and sulfur oxides. Metal / insulator / semiconductor structures with catalytically active gates are widely used to electronically detect the presence of various chemical species [Spetz 2001]. The wide bandgap semiconductor silicon carbide, SiC, enables device operation to temperatures in excess of 1200 K. In the case of the 6H polytype the energy gap is 3.0 eV, compared to 1.1 eV for silicon. These field-effect devices require a robust dielectric to enable modulation of the semiconductor carrier concentration via an applied gate potential. SiC has a native oxide, SiO_2, which fulfills this need. In addition, SiC is chemically stable in reactive environments making it well suited for sensing applications in harsh environments.

Refractory metal gate SiC devices have been demonstrated for high temperature chemical sensing application by a number of groups [Spetz 2001, Filippov 1999, Hunter 2000, Kim 2001, Nakagomi 2001, Samman 2000, Serina 2001, Ghosh 2002]. These include hydrogen and hydrocarbon sensors operating at temperatures from 600 K to 1300 K. Specific sensor configurations have achieved millisecond time response and sensitivity at the 0.1% level. The fast response makes the sensors suitable for feedback control. In addition, there are preliminary indications that suitably designed devices may offer sensitivity to ammonia, carbon monoxide, nitrogen oxides and fluorocarbons.

The operation of field-effect devices is dominated by electronic interactions at interfaces. In the case of a metal/insulator/SiC (MISiC) structure, these interfaces are the environment/metal interface, the metal/oxide interface and the oxide/semiconductor interface, which will be studied using a number of spectroscopic techniques. For the SiC sensor technology to fulfill its potential in real world applications the issues of reliability and stability need to be addressed, which requires a detailed experimental study of hydrogen transduction following dehydrogenation at the heated catalytic gate.

A schematic of our catalytic gate SiC field-effect sensor for hydrogen containing species is shown in Figure I.1. Refractory metal gates such as Pt, Pd and Ir can efficiently dehydrogenate long chain hydrocarbons at temperatures above 700 K. Following dehydrogenation at the heated gate, hydrogen diffuses into the structure. For a Si-based catalytic gate sensor operating below 500 K it has been shown that hydrogen gives rise to a polarized layer at the metal/oxide interface [Lundstrom 1976]. This chemically induced polarization charge results in a simple lateral shift of the C-V or current-voltage (I-V) characteristic of the capacitor or Schottky diode sensor, respectively. The magnitude of the voltage shift in these Si based sensors is a measure of the chemically modified metal/semiconductor barrier height. It has been assumed that the same mechanism describes the operation of higher temperature SiC based sensors for hydrogen containing species. At temperatures above 700 K the diffusion time for hydrogen through 100 nm of Pt and 50 nm of SiO_2 is less than 5 μs [Katsuta 1979] and 0.5 ms [Beadle 1985] respectively. We have previously demonstrated via *in-situ* C-V spectroscopy of $Pt/SiO_2/SiC$ sensors at 800 K that oxidizing species affect the electronic properties of both the metal/oxide and oxide/semiconductor interfaces [Tobias 2003A].

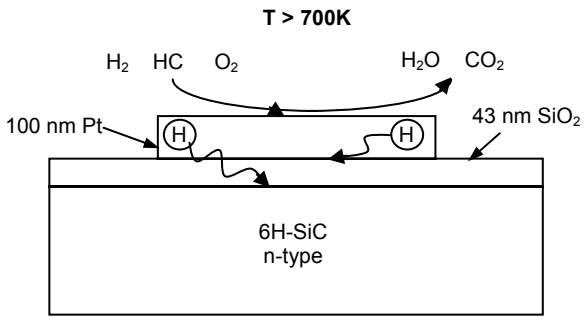

Fig. 1.1 Schematic of a catalytic gate SiC field-effect sensor for hydrogen containing gases. Typical operation is at T > 700 K. Hydrogen can diffuse to both the metal/oxide and oxide/semiconductor interfaces.

2. EXECUTIVE SUMMARY

A silicon carbide (SiC) based sensor for the detection of power plant combustion products has been developed. The sensor is a catalytic gate field effect device that can detect hydrogen containing species in chemically reactive, high temperature environments.

High-temperature reliability is crucial for practical sensor applications. A primary failure mode of SiC devices for power applications is oxide breakdown caused by electron injection from the substrate. Monitoring the gate leakage current as a function of time, temperature and electric field is a standard technique used to determine mean-time-to-failure of metal-oxide-semiconductor (MOS) structures. We have investigated the high-temperature reliability of *n*-type SiC MOS sensors by monitoring the gate leakage current as a function of temperature. We have measured devices made on both the 4H and 6H polytypes of SiC at temperatures up to 600 K and electric field strengths up to 0.6 MV/cm. This electric field is small compared to those usually encountered in power applications, but is appropriate for our sensors, since we have determined that the optimum bias for gas sensing is near midgap. We find leakage current densities below 17 nA/cm^2 at 600 K and below 3 nA/cm^2 at 450 K. These are promising results for high temperature operation.

We have fabricated new sensors with an extra anneal in nitric monoxide that is believed to reduce defect densities further at the interface between the insulator and SiC, and we will compare samples with and without this treatment to find further improvement of the sensors. New masks and holders for metal depositions have been designed by us and manufactured by our machine shop with tighter tolerances for better-defined sensor gates. We have added one step to our procedure for oxide thickness measurement (via spectroscopic ellipsometry), the fitting of the incident angle with a calibration sample, which has improved the accuracy of the measurements significantly.

Our newly built apparatus for fast sensor measurements has been characterized with laser induced fluorescence (LIF) using different gas flows and different distances between the sensor and the gas outlets, and pictures of the gas exchange have been recorded. We found the exchange of the gas environment of a sensor to be complete in one millisecond, for a flow of 400 mL/min and a distance of 0.9 mm. A small distance was found to be most critical for a fast and complete gas exchange.

In collaboration with Dr. Benjamin Chorpening we will be testing our gas sensors in a small scale lab environment at the NETL facility in Morgantown, WV. The B3 reactor has been chosen for the first experiments. We have designed a sensor test module that is compatible with the B3 reactor, and identified specific vendors who can supply the necessary high temperature electrical cabling. The software for running the sensor tests in an industrial environment has been written and tested.

Techniques have been developed for studying the surface chemistry of the platinum gate with Auger electron spectroscopy and temperature programmed desorption, and for reproducibly cleaning the metal surface. Preliminary studies of sulfur adsorption show that the surface can become coated with sulfur by exposure to hydrogen sulfide gas. Such a sulfur coating would probably deactivate the sensor. Attempts to remove the sulfur chemically by exposure to oxygen or hydrogen have so far been unsuccessful, but we attribute this to interference from background CO in the vacuum chamber, which prevents oxygen adsorption on the surface. Introduction of a direct gas dosing system will permit more meaningful studies of the surface chemistry. In addition, new samples have been fabricated that will permit sensor response measurements and surface chemistry studies to be carried out simultaneously *in situ* under UHV conditions.

From a project management perspective, a new postdoctoral researcher, Dr. Yung-Ho Kahng, began work on the surface science program at Tufts University in July 2004. Dr. Kahng has a Ph.D. in experimental condensed matter physics from the University of Massachusetts, Amherst. Michigan State University has posted an advertisement on the AIP server to recruit new candidates for a postdoctoral research associate. We are in the process of evaluating and interviewing candidates. In the meantime, Dr. Peter Tobias, the postdoctoral researcher who was previously working on the project, has continued with the project during the current reporting period. Dr. Tobias is currently searching for a permanent industrial position and plans to continue with the project on a month by month basis.

Four oral presentations were made during this reporting period. Dr. Ruby Ghosh made two conference presentations: (1) “High temperature SiC chemical sensors: an in-situ study of gas response mechanisms” at the 2003 International Symposium on SiC and Related Materials, Oct 5 - Oct 10, 2003 in Lyon, France and (2) "High Temperature Operation of SiC Electronics and Sensors" at the 2004 Electronic Materials Conference, June 23 -25, 2004, University of Notre Dame, South Bend IN. In addition Dr. Ghosh was invited to present the physics colloquium at Auburn University on Jan. 23, 2004. Dr. Peter Tobias presented a paper entitled “Sensing mechanisms of SiC devices for exhaust gas applications” at the second IEEE International Conference on Sensors, Oct 21 - 24, 2003 in Toronto, Canada. His paper was presented in a special session on “Extreme Environment Chemical Sensors” organized by Dr. Ghosh.

3. EXPERIMENTAL

3.1 Samples

For our high temperature sensors, we prepare silicon carbide based metal-insulator-semiconductor devices (MISiCs) as capacitors. The cross section of the finished capacitors is shown in Fig. 3.1.1. The SiC wafers are obtained commercially from Cree, Inc. [Cree]. The thermal oxide is prepared by Cree, Inc. or by the group of J. Cooper at Purdue University. The oxide is grown at Cree in dry oxygen at 1470 K [Lipkin 1996], and at Purdue in wet oxygen at 1420 K, followed at both locations by a wet anneal at 1220 K. The samples are then sawed into 1 cm x 1 cm pieces. While being sawed, the samples are protected with photoresist that is afterwards removed with Nanostrip©. The sample are then covered with photoresist only on the front side, the back oxide is etched off in buffered hydrogen fluoride solution, and the photoresist is removed with Nanostrip©. All chemicals used are CMOS grade.

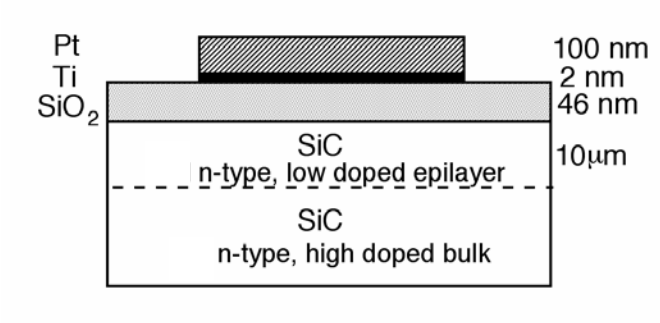

Fig. 3.1.1 Schematic cross section of a MISiC capacitor. Pt is deposited on a thermally oxidized SiC substrate with dot diameters from 200 to 1000 μm. Some samples had an intermediate layer of Ti. The Pt thickness was 100 nm for the sensor and capacitance measurements.

3.1.1 Fabrication of new samples

Some of our old samples had a high density of electronic defects at the interface between the silicon carbide and the silicon dioxide interface, and we had found that these defects lead to a slower signal of the sensors made from this material. It is now generally believed that the defect density can be reduced by an NO anneal after oxidation. We have begun a cooperation with the group of Prof. Williams at Auburn University that uses NO anneals in their processing of silicon carbide samples.

To let us compare samples with different processing, the group of Prof. Williams has oxidized 8 samples of silicon carbide with an NO anneal and 2 without the NO anneal. Additionally, they have oxidized silicon carbide samples with an NO anneal and metallized them with platinum directly afterwards, using their standard process. This allows us to compare their metallization with ours and their effect on the defect density, to see e.g. if the kind of metallization or time between oxidation and metallization strongly influences the samples' properties, as suggested by Prof. Williams.

The thickness of our samples' oxide has been routinely measured with a spectroscopic ellipsometer by JA Woollam Co., Inc. with wavelengths covering the whole visible spectrum. To check the precision of the ellipsometer and to improve the accuracy of the measurement, we bought a calibration sample from Gaertner Scientific. We remeasure its oxide thickness of 51.2 nm each time we measure the oxide thickness of a silicon carbide sample. The fitting of the ellipsometer's program with the calibration sample turned out to be very important, because without it the measured thicknesses in some cases would have been too large by a whole nanometer.

For the metallization of our samples, we designed new sample holders and shadow masks. The old masks and holders had some shortcomings:

- The masks were lacking markers to identify with which mask a sample had been processed;
- The outer dimensions of masks and holders had too large tolerances. Masks that move in the holders during the metal deposition lead to badly defined metal dots;
- The smallest holes in the mask were larger than planned due to the difficult production.

The machine shop of the MSU Physics department cut the new masks and holders with tighter tolerances and made the holes with wire EDM, which for hole diameters of 200 micrometers is not an easy task.

3.1.2 Metal deposition

The interface between the metal and the insulator is critical both for gas sensing and for metal adhesion, which is important for sensor reliability. To get a sharp and reproducible interface, we cleaned the sample prior to metal deposition by the RCA method: We clean the samples in a solution of conc. NH_3, 30%-H_2O_2 and H_2O (1:1:6) at 75 °C for 20 min and, after rinsing with distilled water, then in a solution of conc. HCl, 30%-H_2O_2 and H_2O (1:1:7) at 75 °C for another 20 min. At the end, the samples are

rinsed with distilled water and left in the water until metal deposition. The chemicals used for cleaning are from J.T. Baker, CMOS grade.

After being thoroughly rinsed and blown dry with nitrogen, metal dots are deposited on the front side of the samples through a shadow mask at a temperature of 600 - 650 K. The metal thickness is ~100 nm for the capacitance and sensor measurements. We have used our new shadow masks with dot areas from 3.1×10^{-8} up to 1×10^{-6} m^2, giving us arrays of 50 sensors per SiC chip. The metal was deposited by sputtering in argon at a pressure of 0.33 Pa. The precision of the thickness monitors in the deposition chambers is checked in regular intervals with a Dektak profilometer. Each dot is the gate of a metal-insulator-silicon carbide capacitor (MISiC).

3.1.3 Contact to the metal gates

Electrical contact to the metal gates was made by using an ultrasonic wire bonder from Kulicke and Soffa. The SiC sample was glued to an alumina header with gold pads. Prior to bonding the Pt gates on the SiC substrate were always rinsed with isopropanol (CMOS grade). The sample was heated to 600 K on a hot chuck. Gold wire, 25 μm in diameter, was first bonded to the gold pads on the header then to the Pt capacitor gates. The critical bond is the one made to the Pt gate. For proper adhesion, we found it necessary to bring the tool down on the Pt gate, hold it in place for 10 s, and then apply the ultrasonic power to make the bond.

3.2 Time-resolved fast sensor test assembly

We have continued developing the software and hardware of our measurement procedures so that a person with experience in sensor testing should be able to use the programs intuitively.

3.2.1 Motivation for characterizing the set-up with an independent method

In our last report we presented a new set-up that we built for characterizing fast gas sensors. The gas environment of a sensor in the set-up can be exchanged quickly by moving another gas outlet in front of the sensor. We have studied experimentally the details of the gas exchange in our set-up, especially how fast and how complete it is and on which experimental variables a fast and complete gas exchange depends. In principle, this could be also done theoretically, but to do it experimentally has some advantages:

1) The two gas outlets in Fig.3.2.1 are not smooth on the length scale of the experiment, leading to nonideal boundary conditions and, as will be seen, to turbulent flows. This makes a computational treatment difficult.
2) The movement of the outlets in time was not well enough known beforehand, but is now known as a result of the experiment.
3) While our group has no experience computing gas flows patterns, the research group of Prof. Koochesfahani at Michigan State University routinely measures flow, laminar and turbulent, with many different boundary conditions.

Our problem aroused the scientific curiosity of Prof. Koochesfahani sufficiently that he was willing to collaborate with us in characterizing our set-up.

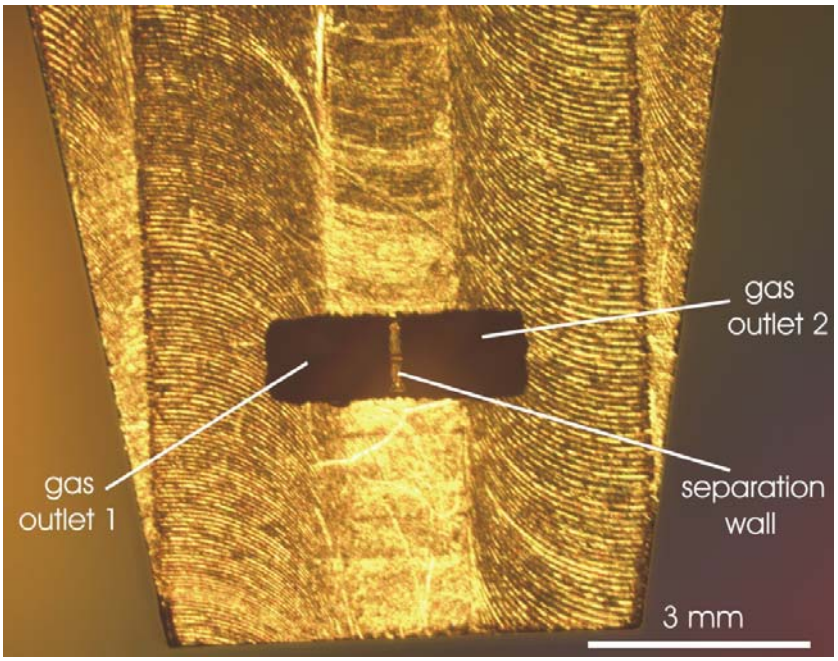

Fig. 3.2.1. Photo of the moving gas outlets (MGO) as they were used in the characterization of the fast sensor test assembly. The two outlets move sideways by 3 mm.

3.2.2 Characterizing the set-up with laser induced fluorescence (LIF)

The group of Prof. Koochesfahani at Michigan State University studies gas flows by molecular tagging techniques. A gas is tagged by the addition of a gas like acetone that fluoresces in ultraviolet light: An ultraviolet photon is exciting the acetone molecule that in turn is sending out a photon in the blue-green range that passes the filter of a camera that takes the picture. When one gas is tagged, its molecules carry the acetone molecules along, and it appears therefore blue upon UV illumination, while another gas that is not tagged will appear dark [Lozano 1992]. In our experiments, two gases, one tagged and the other untagged, stream from different sources into a common space, and pictures of the fluorescence light during a high intensity pulse of UV illumination reveal the location and sharpness of the boundary between the two gases. One gas is pure nitrogen, while the other gas is nitrogen to which acetone is added, about 15 percent. The total gas flows out of the two outlets were equal to each other in this and all the other experiments. An acetone molecule fluoresces blue when a UV light pulse from an argon laser that has a wavelength of about 308 nm hits it, see Fig. 3.2.2a.

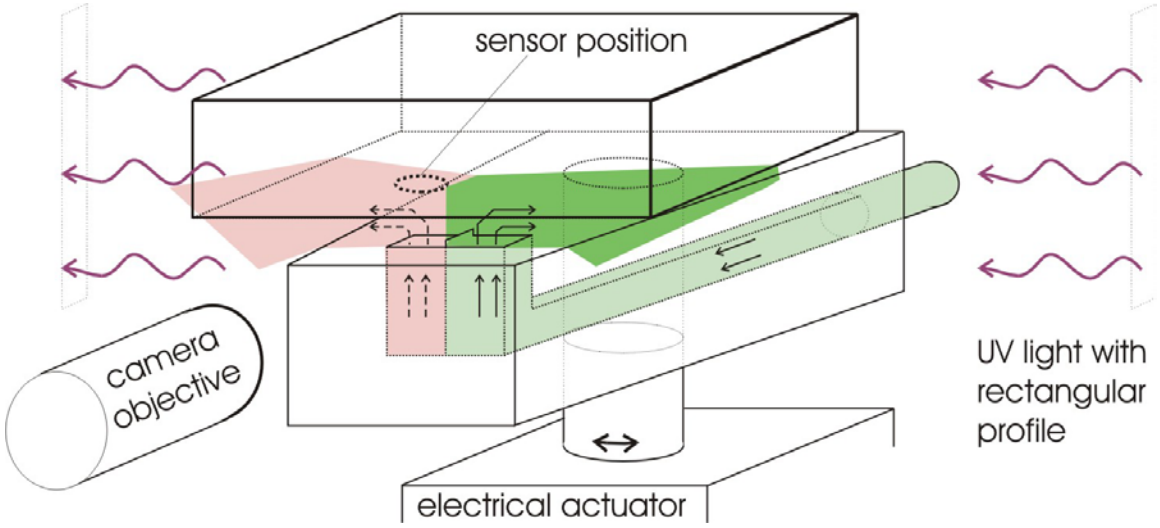

Fig. 3.2.2a. Set-up for fast sensor measurements, characterized by laser induced fluorescence. The gas out of the right outlet is tagged with acetone and fluoresces upon UV illumination.

In our first experiment, we use two gas flows streaming out of the moving gas outlets (MGO), without hitting a plate above the outlets. The gas is streaming from the MGO in a homogeneous jet upward. The boundary between the two gases is straight and doesn't show signs of turbulence.

In our second experiment, we placed a quartz plate above the MGO, as shown schematically in Fig. 3.2.2a, where we would place our SiC sensor, to simulate the effect of the planar sensor on the gas flows. The gas is first streaming upwards and is then forced by the quartz plate and the second gas stream to flow to the side opposite to the other gas stream. The boundary between the two gases is nearly straight; at the wall between them, there develop only small turbulences see Fig. 3.2.2b.

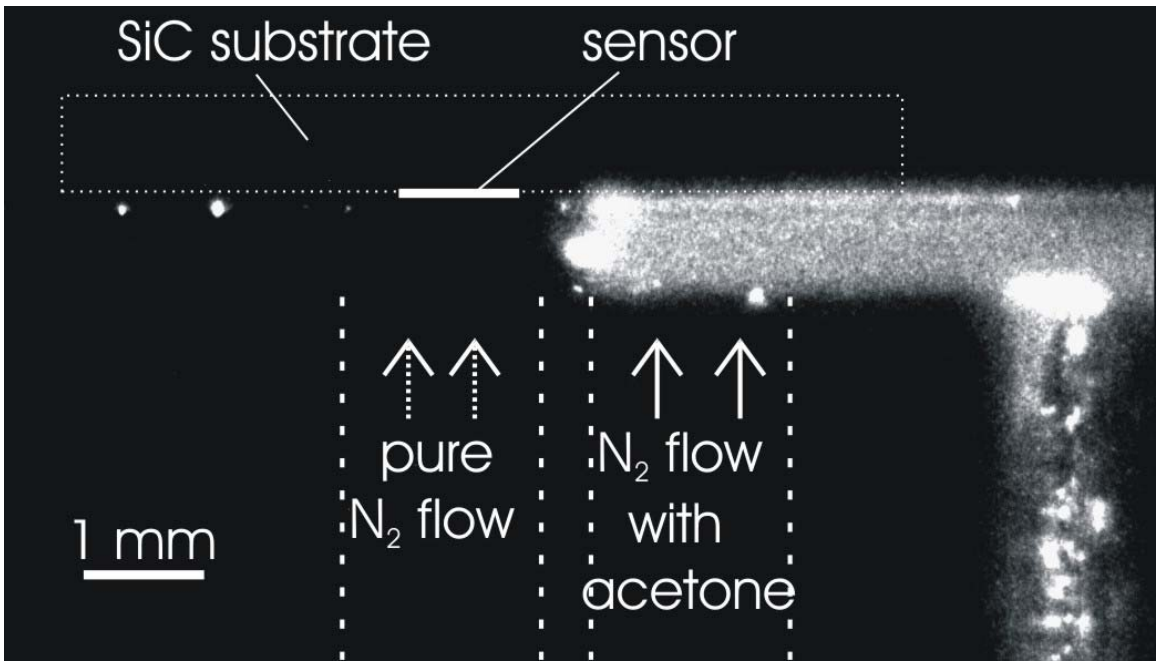

Fig.3.2.2b. Laser induced fluorescence image of the set-up, demonstrating that the two gas flows don't mix. Nitrogen flows out of each outlet at 370 ml/min, with fluorescing acetone in one of the two flows. 1 mm above the outlets, a horizontal plate forces the gases to flow to the sides, as would our SiC sensor. The position of the sensor is indicated. Note that the overexposed bright spots are not fluorescence from the acetone, but from scattered light.

In the third experiment, we have the same set-up as in the second, but move the MGO, as we would do in studying a fast gas sensor. The electronic circuit, described in the last report, gives an electrical pulse to the actuator that moves the MGO and, at the same time, gives a trigger pulse to the camera system to define the time zero. The camera takes pictures of the two gases and their boundary at different times after the electrical pulse. Fig. 3.2.2c shows how the boundary between the two gases is following the movement of the MGO with a delay of about a millisecond.

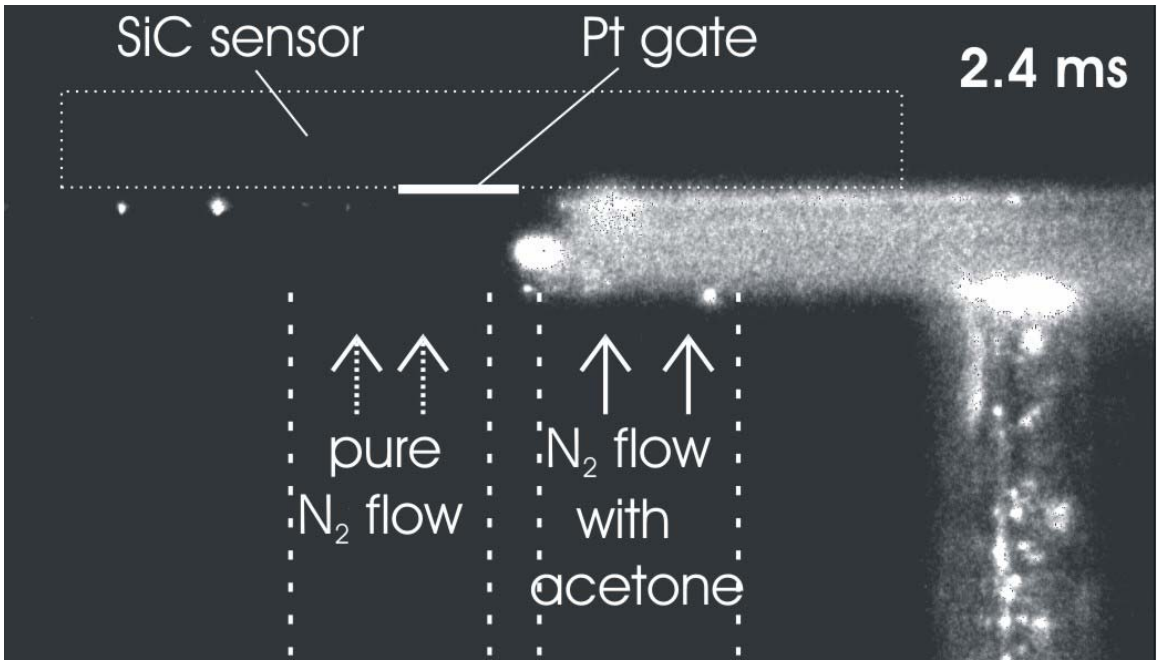

Fig. 3.2.2c. Laser induced fluorescence image of the set-up, 2.4 ms after the trigger pulse. The outlets have started moving to the left, the boundary between the two gas streams closely follows.

From a series of such pictures taken at different times, we estimated how fast and how complete the gas exchange is. We have investigated how the gas flow and the distance between outlets and quartz plate influence the exchange of gases by taking pictures while using gas flow rates out of one outlet of 100 and of 400 mL/min and distances of 0.8 and 1.3 mm. The third experiment provided us also with the information about the movement of the MGO when powered with our electronics; the reference point of the MGO movement in the pictures was the reflected spot of the separation wall between the outlets.

In the experiments, we frequently changed out of which of the two outlets the tagged gas would exit, while the untagged gas would exit out of the other hole, respectively. We also took pictures of the MGO moving in either direction. We didn't find significant difference between the two outlets in the MGO or between the two directions of movements of the MGO, our set-up appears to work nearly symmetrically.

In a control experiment, tagged gas was coming out of both outlets, with the pictures showing us that the gases from the outlets efficiently pushed away all laboratory air from the space above the moving gas outlets and the intended sensor position.

3.3 Sensor measurements at the National Laboratory in Morgantown

We plan to make measurements with our sensors in the gas flow of the test reactor B3 in the National Laboratory in Morgantown, where realistic conditions of high temperature sensor applications can be simulated. We have designed a sensor mounting that should withstand the rough conditions of such a measurement, especially high

temperatures, mechanical vibrations and electromagnetic interference. Fig. 3.3 shows schematics of the set-up with dimensions and part numbers. The gas flow in the B3 reactor is led through the Swagelok union tee.

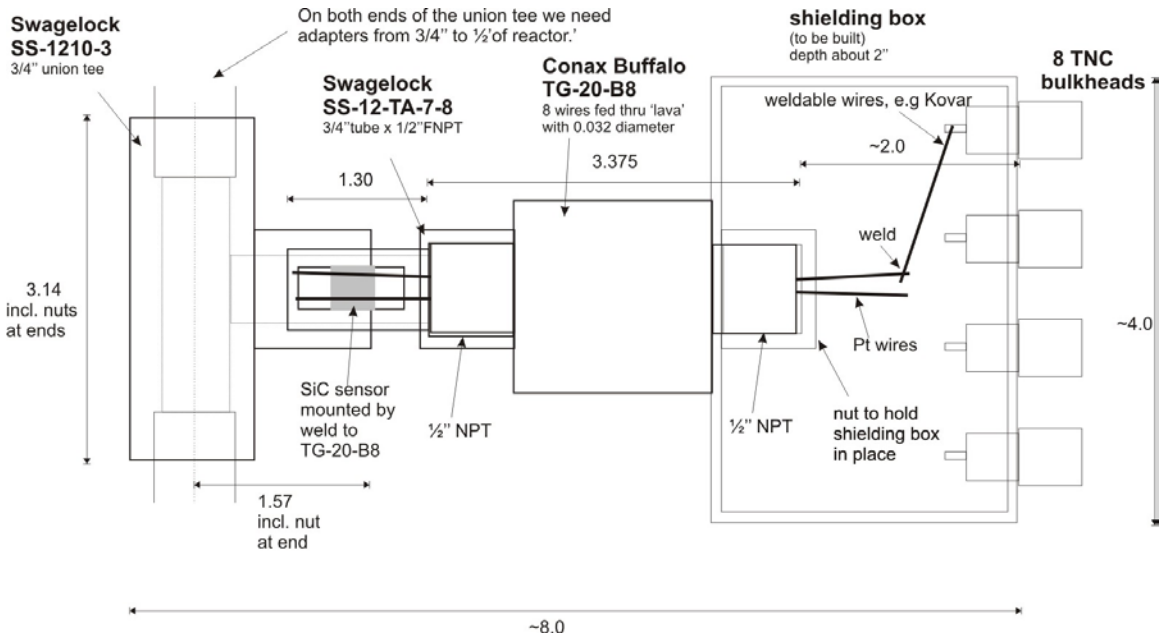

Fig. 3.3. Design of measurement set-up for sensor measurements in National Laboratory in Morgantown.

The SiC sensor is mounted on an alumina header with many Au contact pads. For contacting the sensors, we will bond 25 μm Au wires between the Pt gates and Au pads. Fifty μm Au wires will be bonded to the Au pads on one side and wrapped around thick Pt wires on the other side, where they are additionally secured with colloidal silver paste. The Pt wires in turn will be welded to Kovar wires, which will also be used for the center conductor contacts of our coaxial cables. We surround the sensor and all conductors with conducting metals to protect the capacitance measurements of our sensors from electromagnetic interference.

3.4 Leakage current measurements

MOS device operation in chemically corrosive, high temperature environments places stringent demands on the stability of the insulating dielectric and the constituent interfaces within the structure. The primary mode of oxide breakdown under these conditions is attributed to electron injection from the substrate. Measurements of gate leakage current as a function of electric field, temperature and time is a standard technique used to determine mean-time-to-failure for MOS devices. The reliability of n-

type SiC MOS sensors was investigated by monitoring the gate leakage current as a function of temperature.

The refractory metal gate SiC MOS devices (see Fig. 3.1.1) were fabricated on commercially available highly doped (1 - 11 × 10^{18} N/cm^3) n-type wafers with a low doped (1 - 2 × 10^{16} N/cm^3) 3 - 5 μm epitaxial layer. Both the 4H and 6H polytypes were used. The specific details of the samples used for the high temperature gate leakage measurements are given in Table 3.4. The wafers were cut into 1 cm squares and stripped of the native oxide. An oxide 40 - 50 nm thick was grown on the square samples via either a "wet/reox" or "dry/reox" process. "Wet/reox" refers to oxidation 1150°C in wet O_2, followed by an *in-situ* Ar anneal and wet reoxidation at 950°C whereas "dry/reox" refers to dry oxidation at 1200°C, followed by a 950°C wet reoxidation [Lipkin 1996]. The precise oxide thickness was determined by spectroscopic ellipsometry.

The interface between the gate metal and the dielectric is critical for both metal adhesion and gas sensing. Prior to metallization the samples were cleaned in two RCA solutions in a class 100 cleanroom. First we use a solution of conc. NH_3, 30%-H_2O_2 and H_2O (1:1:6) at 75 °C for 20 min and a distilled water rinse, followed by a solution of conc. HCl, 30%-H_2O_2 and H_2O (1:1:7) at 75 °C for another 20 min. After a long rinse in distilled water the samples were stored in DI water until immediately prior to metal deposition. The CMOS grade chemicals were obtained from J.T. Baker. Arrays of circular Pt or Ti/Pt dots, ranging in diameter from 50 to 1000 μm, were e-beam evaporated or sputter deposited through a shadow mask. In the case of the sputtered samples the base chamber pressure was 3 × 10^{-8} Torr, and Pt was sputtered at 350°C in a 5 mTorr Ar atmosphere. The e-beam samples were also evaporated at 350°C in a 10^{-8} Torr chamber. The nominal gate thickness was 100 nm. One of the samples used for the gate leakage measurements was only 15 nm thick, it was originally designed for a related photoemission experiment [Tobias 2003B].

A common back contact to the entire array of devices on the 1 cm^2 sample was made by stripping off the back oxide in CMOS grade buffered HF, then attaching the sample with a conducting silver paste onto an alumina header with gold pads. Electrical contact to the Pt gates was made with Pt probe tips for the leakage measurements. For capacitance - voltage characterization gold wire was bonded at 350°C between the Pt gate and the gold pads on the alumina header.

Sample	bulk doping (x 10^{18} N/cm^3)	Epitaxial layer		Gate Oxide		Gate Metal	
		doping (x 10^{16} N/cm^3)	thickness (μm)	growth technique	thickness (nm)	type	thickness (nm)
6H-1	1.01	2.1	3	wet/reox	49.2	sputtered Ti/Pt	2/100
6H-2	1.01	2.1	3	wet/reox	47.2	sputtered Pt	15
4H-1	11.0	1.3	5	dry/reox	49.4	sputtered Pt	100
4H-2	11.0	1.3	5	dry/reox	40	e-beam Pt	100

Table 3.4. Details of the four different samples used to investigate high temperature sensor reliability. The SiC bulk and epitaxial layers are all n-type (doped with nitrogen). Two oxidation processes were used: "dry/reox" and "wet/reox" (see text for details). A cross sectional view of an individual sensor is shown in Fig. 3.1.1.

The gate leakage measurements were made in air using a commercial current - voltage characterization system [Keithley]. The samples were placed inside a shielded probe station with a temperature controlled chuck that can be heated up to 330 °C. To make ±2 pA measurements at high temperature, care was taken to electrically isolate the SiC sample mounted on its alumina header from the heater coils of the hot chuck. At a given temperature both a current - voltage (I-V) and capacitance - voltage (1 MHz C-V) scan were taken for each device. The gate leakage characteristic as a function of gate voltage was obtained by subtracting out the "probe up" current. The midgap voltage was obtained by calculating the midgap potential from $1/C^2$ analysis of the C-V characteristic in depletion.

For sensor measurements in hydrogen and oxygen the devices were characterized via capacitance-voltage (C-V) spectroscopy in a furnace with a controlled gas atmosphere. Contact to the Pt sensing gate was made by bonding an additional gold wire to the gold pad on the alumina header, then attaching the far end of the gold wire to the center conductor of the coaxial cable leading out of the furnace. In our sensor testing system we can make four-terminal electrical measurements with pA and pF sensitivity up to temperatures of 600°C. A commercial measurement setup was used to obtain the 1 MHz C-V characteristics in hydrogen and oxygen [Keithley]. The ambient gas in the furnace tube can be controlled to the ppm level. Measurements were made using 99.999% purity pure nitrogen, mixtures of 10.3 % hydrogen in nitrogen, or 99.99% purity mixtures of 1.0 % oxygen in nitrogen. Typical gas flow rates were 400 ml/min.

3.5 UHV surface chemistry

Much effort during this reporting period has been devoted to the fundamental methods and measurement techniques that are necessary for meaningful and reproducible surface chemical measurements on Pt/SiO_2/SiC samples. These include mounting the sample in a way that is compatible with ultrahigh vacuum (UHV) and able to withstand repeated thermal cycling between 200 K and 1000 K; reliable temperature measurement

and control over that range; *in situ* cleaning of the Pt surface to obtain a reproducible, atomically clean surface, and methods for measuring temperature-programmed desorption signals.

Preliminary experiments have been carried out to investigate sulfur adsorption on the surface of the Pt gate and the possible reactions of the adsorbed sulfur with oxygen.

All of the UHV experiments to date have been carried out on a $Pt/SiO_2/SiC$ sample with a single large (1 cm^2) gate that was fabricated at MSU several years ago using essentially the same gate metallization methods that are currently in use. We have also designed a new gate pattern suitable for combined *in situ* surface analysis and sensor response measurements in UHV. Four new $Pt/SiO_2/SiC$ samples have been fabricated, which will be used in the coming year.

3.5.1 Sample mounting and thermometry

The $Pt/SiO_2/SiC$ sample was mounted to an alumina header that was commercially screen-printed with gold electrical contacts according to our design [Piconics]. The sample was bonded to the header with colloidal silver paste. Both sample and header were cleaned with methanol prior to mounting (for future samples intended for capacitance measurements, CMOS-grade isopropanol will be used). The assembly was baked in air on a hot plate at 200 - 300°C before being loaded into the UHV chamber. We have determined that this mounting system withstands multiple (>20) heating and cooling cycles between 200 K and 1000 K without failure; does not outgas appreciably during heating, and provides excellent thermal contact between the header and the sample.

Silver paste was also used to bond a fine-wire Type K thermocouple to the front of the sample for temperature measurements. (In UHV measurements, where the ambient gas density is so low that its thermal conductivity is negligible, the sample is far from thermal equilibrium with its environment, so it is essential that the thermometer be mounted directly to the surface of the sample. Mounting the thermocouple to the header, for example, could give erroneous results.) This bond has also remained intact through multiple heating/cooling cycles, and comparison of carbon monoxide temperature-programmed desorption measurements with published data indicates that the measured temperature deviates from the actual surface temperature by less than 50 K. These results are discussed in greater detail in section 4.3.1.

3.5.2 Surface cleaning

Reproducible surface chemistry measurements require the ability to prepare an atomically clean surface *in situ*. Surface cleanliness is generally determined with Auger electron spectroscopy (AES), which measures the energies of secondary electrons emitted from the surface when it is bombarded with high energy (2 keV) electrons. The energies are characteristic of the specific elements present on or near the surface. The primary contaminants on the Pt surface are carbon, sulfur and oxygen. The upper curve in Fig. 3.5.2 shows an AES spectrum of a sample contaminated with sulfur and carbon. The contaminants are removed primarily by sputtering in 5×10^{-5} Torr Ar at 850 K for 40 minutes followed by annealing to 1000 K to restore surface order. Sputtering always

leaves a small amount of carbon on the surface, however, due to unavoidable CO in the sputtering gas. This residual carbon is removed by heating the sample at 800 K in 1.5×10^{-7} Torr oxygen for 30 minutes. The lower curve in Fig. 3.5.2 shows an Auger spectrum of the sample after cleaning; no peaks other than those attributable to Pt are detectable. (Note that the peak near 150 eV includes contributions from both Pt and S; the intensity of that peak relative to the other Pt peaks in the lower spectrum is characteristic of clean Pt.)

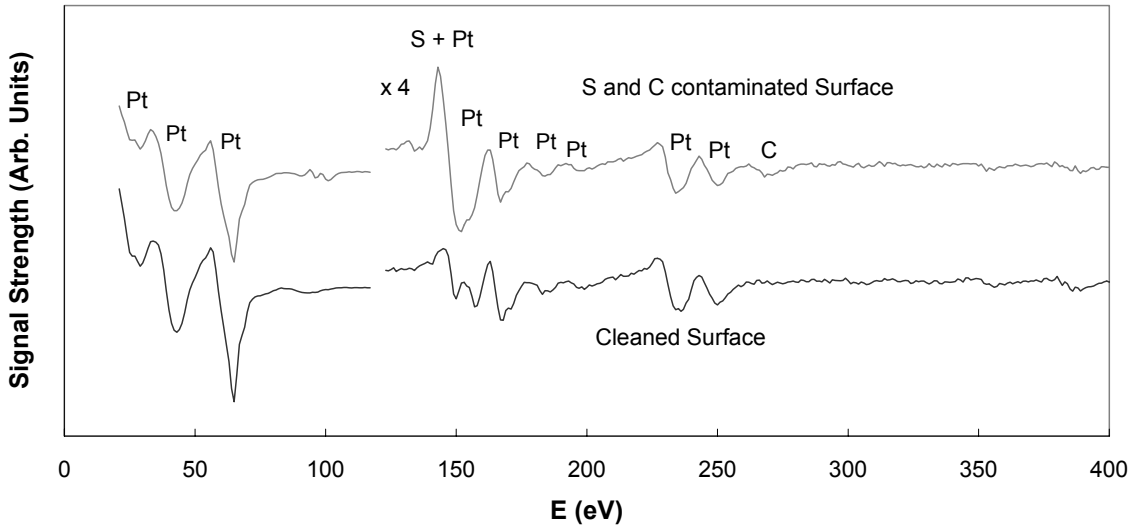

Fig. 3.5.2. Auger spectra showing sample cleaning, with peaks due to contaminants highlighted. The upper curve shows the spectrum for the Pt gate contaminated with sulfur and carbon. The lower curve shows the spectrum of the same surface after argon ion sputtering and heating in oxygen. Note that the peak at 270 eV due to carbon is eliminated. The peak at 150 eV has contributions from both Pt and sulfur; the peak intensity in the lower curve is characteristic of clean Pt.

3.5.3 Temperature programmed desorption

Temperature-programmed desorption (TPD) is a standard technique in surface chemistry for measuring adsorbate surface coverages, binding energies, and for identifying and characterizing surface chemical reactions. The sample is exposed to one or more gases at a sufficiently low temperature (typically ~100 K) that the gases stick to the surface and do not react. The sample is then heated at a linear rate, $dT/dt \sim 5$ K/s, and the gases evolved from the surface are detected with a quadrupole mass spectrometer (QMS).

In our last technical report (41847R01) we described an interaction between the electron-beam system used for heating the sample and the QMS, which produced spurious signals, and we demonstrated a normalization procedure that reduced the

interference, but at a cost in sensitivity and speed of data acquisition. In the current reporting period we have developed and tested a shielding system that reduces the spurious signals to an acceptable level.

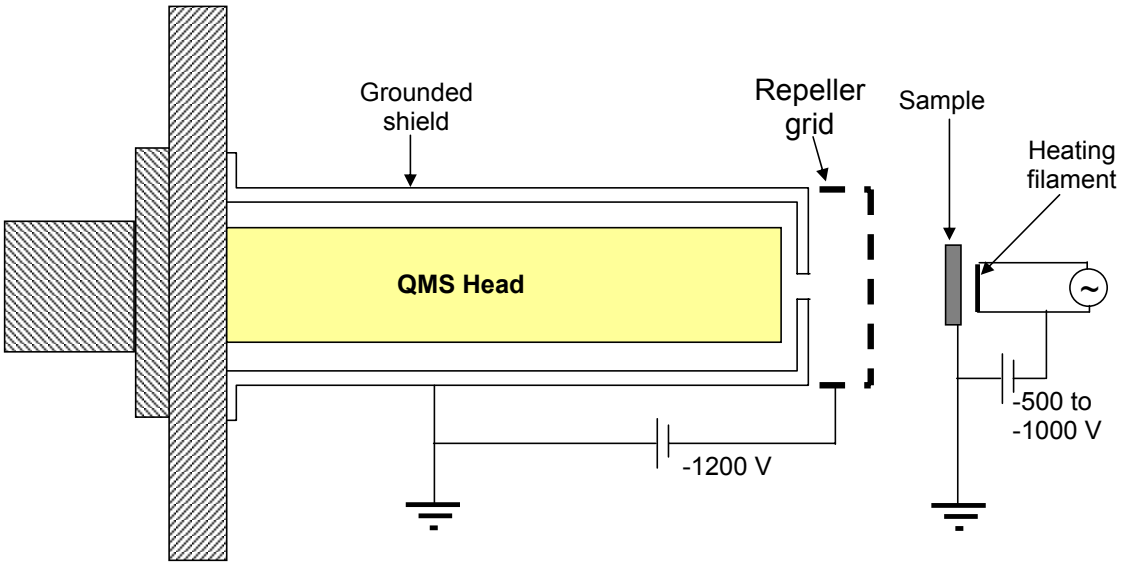

Fig. 3.5.3a. Schematic diagram of the electrostatic shield and negatively biased repeller grid used to prevent stray electrons from the heating filament from entering the QMS head and interfering with TPD measurements.

Fig. 3.5.3a shows a schematic diagram of the system. The QMS head is surrounded by an electrically grounded shield with an aperture facing the sample for the entry of molecules desorbing from the surface. In front of the aperture is an electrically isolated wire grid, which is biased at a high negative potential (typically ~ -1200 V) to repel any negatively charged ions or stray electrons emitted by the heater filament.

Fig. 3.5.3b compares simulated TPD scans measured with no bias applied to the grid and with a bias of -1200 V. In these measurements the masses observed correspond to nonexistent species, so the real signal should be zero. The large spurious signals during heating seen without bias are largely eliminated when the grid is biased at -1200 V.

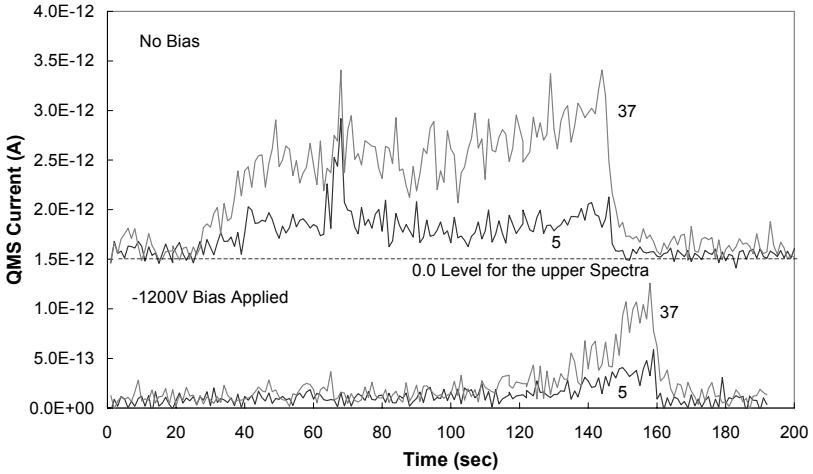

Fig. 3.5.3b. Pressure-time traces measured by the QMS during sample heating, for two masses (5 and 37 amu) at which no real signal is expected. For the upper pair of graphs no bias was applied to the grid, and a strong spurious signal is observed in both mass channels during heating. In the lower traces, a bias of -1200 V was applied, and the spurious signal is dramatically reduced.

3.5.4 Techniques for studying sulfur contamination

Sulfur is frequently present in significant concentrations, usually as H_2S, in practical sensing environments, including those relevant to coal combustion and gasification. Adsorbed sulfur is well known as a "poison" for its ability to eliminate the catalytic activity of transition metals, such as platinum. On the other hand, catalytic oxidation and reduction of adsorbed sulfur can also take place under some conditions, providing self-cleaning of the surface. To investigate the possible effects of sulfur on our sensors, we are developing procedures to study sulfur contamination and removal.

We have shown that sulfur can be reproducibly deposited on the Pt surface in controlled amounts by exposing the sample to H_2S at room temperature. The amount of adsorbed sulfur can be measured with Auger spectroscopy, as illustrated in the upper trace of Fig. 3.5.2. Adsorbed sulfur can be removed by argon ion sputtering as shown by the lower curve of Fig. 3.5.2. Reactions of adsorbed sulfur with other gases can be studied either by heating the sample in the desired gas, followed by Auger spectroscopy, or by TPD, with the two gases coadsorbed at low temperature. In the latter case a reaction is demonstrated by the desorption of the reaction product (e.g. SO or SO_2 from coadsorbed sulfur and oxygen) as well as by changes in the sulfur Auger signal.

3.5.5 Design and fabrication of sensor samples for UHV studies

The UHV studies to date have been carried out on a $Pt/SiO_2/SiC$ sample fabricated several years ago with the 1 cm^2 front surface completely covered with the Pt film. This sample is adequate for surface chemistry measurements, but it is not suitable for *in situ* sensor response measurements, because the gate area is far too large.

Accordingly, four new samples were fabricated at MSU during the current reporting period, using the same materials and cleaning and deposition procedures as for the samples used for sensor characterization, but with a gate pattern optimized for UHV studies. A micrograph of one of the samples is shown in Fig. 3.5.5. The large Pt area in the middle provides a large surface area for standard UHV surface chemistry probes such as Auger spectroscopy and TPD, while the smaller circular areas will act as gates for simultaneous *in situ* capacitance measurements. The samples will be tested and characterized using the sensor test rig at MSU prior to use in the UHV experiments.

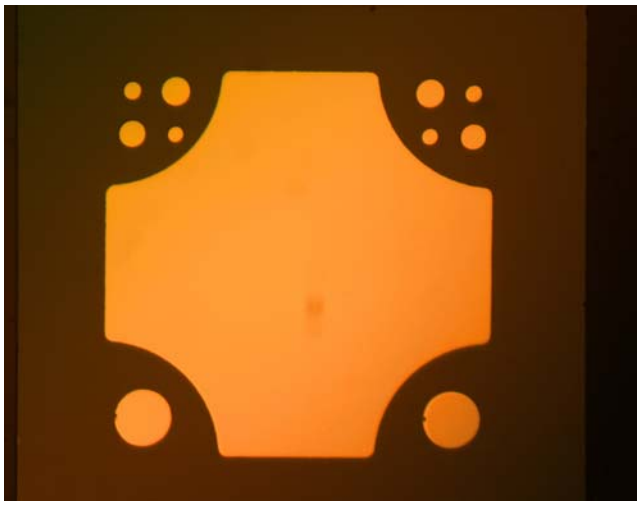

Fig. 3.5.5. Micrograph of sample fabricated for UHV sensor response and surface chemistry studies. The overall sample dimensions are 1 cm × 1 cm, and the circular gates have diameters of 200 μm, 500 μm and 1000 μm. The large Pt area in the center provides a large surface area for surface analysis, while the circular gates will permit *in situ* capacitance measurements.

4. RESULTS AND DISCUSSION

4.1 Characterizing of the set-up with Moving Gas Outlets (MGO)

Fig. 4.1 shows the displacement of the MGO after the beginning of the electrical pulse. It is nearly the same in both directions. The measured displacements are not exactly on one line to give a completely reproducible movement of the MGO after each pulse, but they are sufficiently close to a line to be reproducible within 0.1ms.

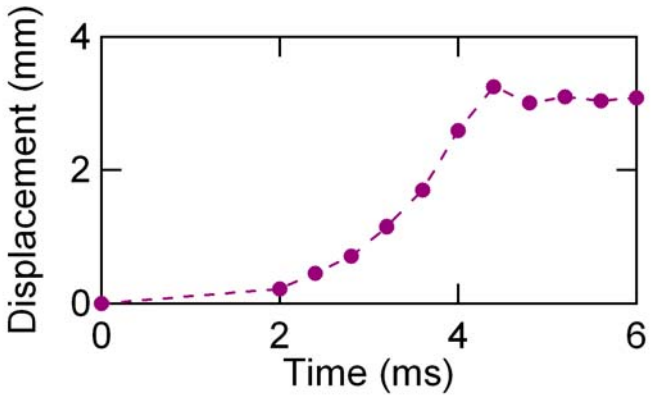

Fig 4.1. Displacement of the moving gas outlets in time, with the rising edge of the actuator voltage being t = 0 ms. The actuator is one of the fastest available.

From pictures series like the one from which Fig. 3.2.2c is taken, we can estimate the speed and completeness of the gas exchange at the location of the sensor. Within the accuracy of our measurements, the gas exchange in our set-up is complete: When the sensor is positioned above one outlet, none of the gas of the other outlet reaches the sensor. If the gas from the other outlet is fluorescing, the region under the sensor is as dark as the noise level, and if gas A is fluorescing, the region under the sensor is as light as the region directly above the outlets, which serves as reference for the correlation between brightness and gas concentration. This was seen for different values of gas flows and of the distance between sensor and gas outlets.

We investigated the influence on the speed of the gas exchange of the two parameters that seem most important, namely the size of the gas flow out of each outlet and the distance between sensor and outlet. The first was found less critical in the investigated range while the latter was found of paramount importance.

Our best parameters were a flow of 400 mL/min out of each outlet and a gap width between sensor and gas outlet of 0.9 mm. Our set-up for characterizing fast gas sensors reaches the planned goal of exchanging the gas environment of a planar sensor with one millimeter diameter within one millisecond. All traces of the old gas environment have disappeared in another millisecond. For sensors with smaller diameter, the gas exchange is faster.

4.2 High-temperature reliability studies

4.2.1 Optimum sensor operating point

SiC MOS device operation in chemically corrosive, high temperature environments places stringent demands on the stability of the insulating dielectric and the constituent interfaces within the structure. The primary mode of oxide breakdown at elevated temperatures is attributed to electron injection from the substrate [Maranowski 1998, Dimitrijev 2003]. The band alignment between SiO_2 and different polytypes of SiC as well as Si has been investigated using internal photoemission techniques [Afanas'ev 1996]; their results are summarized in Fig. 4.2.1.

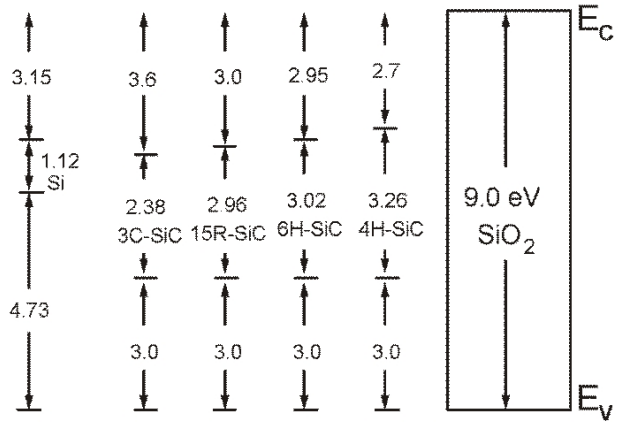

Fig. 4.2.1. Band alignment of the interface between SiO_x, Si and SiC, showing the conduction band offset between the various semiconductors and SiO_2 [Afanas'ev 1996].

At present the majority of SiC devices are fabricated on 4H and 6H substrates due to the commercial availability of these wafers. Both 4H-SiC and 6H-SiC have a larger band gap than Si. However, as Fig. 4.2.1 shows, the alignment of the conduction bands is such that there is actually a smaller barrier towards electron injection from the conduction band of the semiconductor into the insulator for these two SiC polytypes than in the case of Si. To minimize the deleterious effects of oxide breakdown it would be advantageous to operate the MOS device in a regime where the electric field across the oxide is minimized. For our n-type SiC MOS structures biased at midgap, we measure electric field strengths below 0.6 MV/cm at temperatures up to 600 K. Therefore we postulate that the optimum sensor operating point with respect to long term device reliability at high temperatures is at midgap.

4.2.2 Gate leakage current measurements at high temperature

The gate leakage current as a function of gate voltage and temperature was measured from room temperature to 600 K in laboratory air. Only the higher temperature

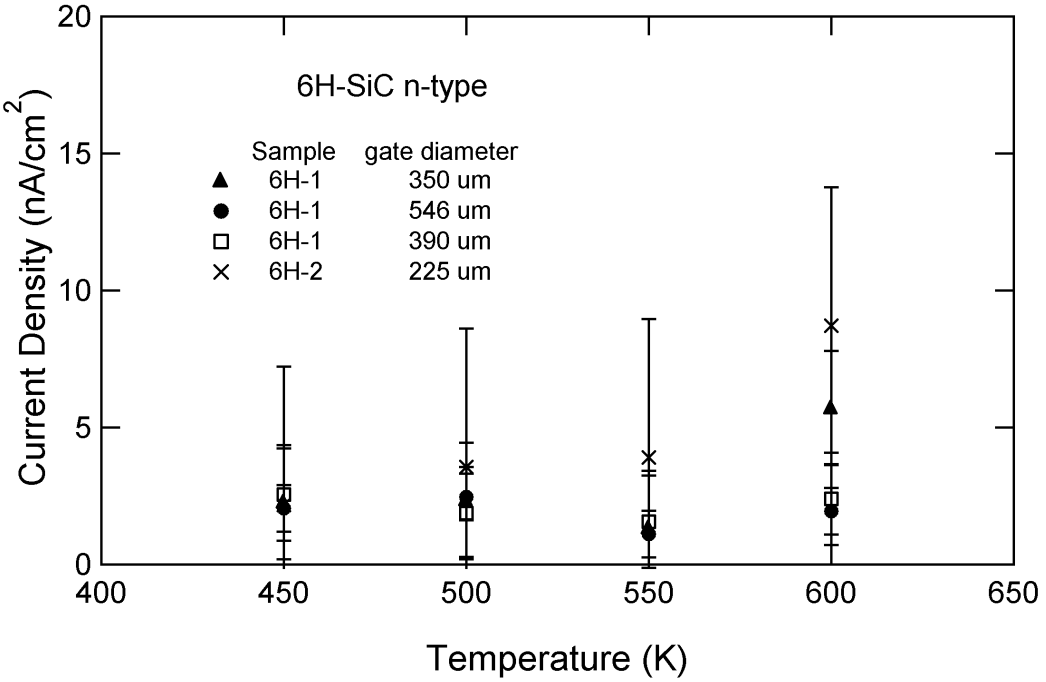

Fig. 4.2.2a. Gate leakage current density as a function of temperature for 6H-SiC n-type devices. See Table 3.4 for details of the device geometry. The capacitor is biased at midgap to optimize device reliability at high temperature.

results above 450 K are shown in Figs 4.2.2a and 4.2.2b. The current density was evaluated at the midgap gate bias. The current densities for four different gates, fabricated on two separate 6H-SiC samples and from three gates fabricated on two different 4H-SiC samples are shown in Figs 4.2.2a and 4.2.2b respectively. The error bars in both figures do not reflect the device quality, rather they are due to the ±2 pA measurement uncertainty on the hot chuck. Below 500 K the leakage current is approximately constant and begins to increase between 550 and 600 K. Note that the electric field across the oxide at midgap for all the devices is low, <0.6 MV/cm up to 600 K. Within our small measurement set, no correlations between gate diameter, metallization technique or gate material, oxidation method or oxide thickness were observed.

Two groups have recently reported on the reliability of "state of the art" thermal oxides grown on n-type 4H-SiC substrates. MOS capacitors with mean time to failure of >10 hours at field of 7 MV/cm at 570 K were observed [Das 2004]. Room temperature measurements of leakage current densities below 1 nA/cm^2 for oxide fields up to 6.5 MV/cm have also been reported [Senzaki 2004]. An important difference between our devices and the gate oxidation process used by both these groups is the addition of a high temperature nitridation process immediately following dry thermal oxidation, which has been shown to significantly decrease the interface state density near the conduction band edge of 4H-SiC. For n-type 6H-SiC MOS capacitors operating at 725 K, current densities <100 nA/cm^2 (for oxide fields up to 8.9 MV/cm) and a 12 MV/cm dielectric breakdown strength have been reported [Wang 2000]. The gate dielectric of these devices included a SiN layer.

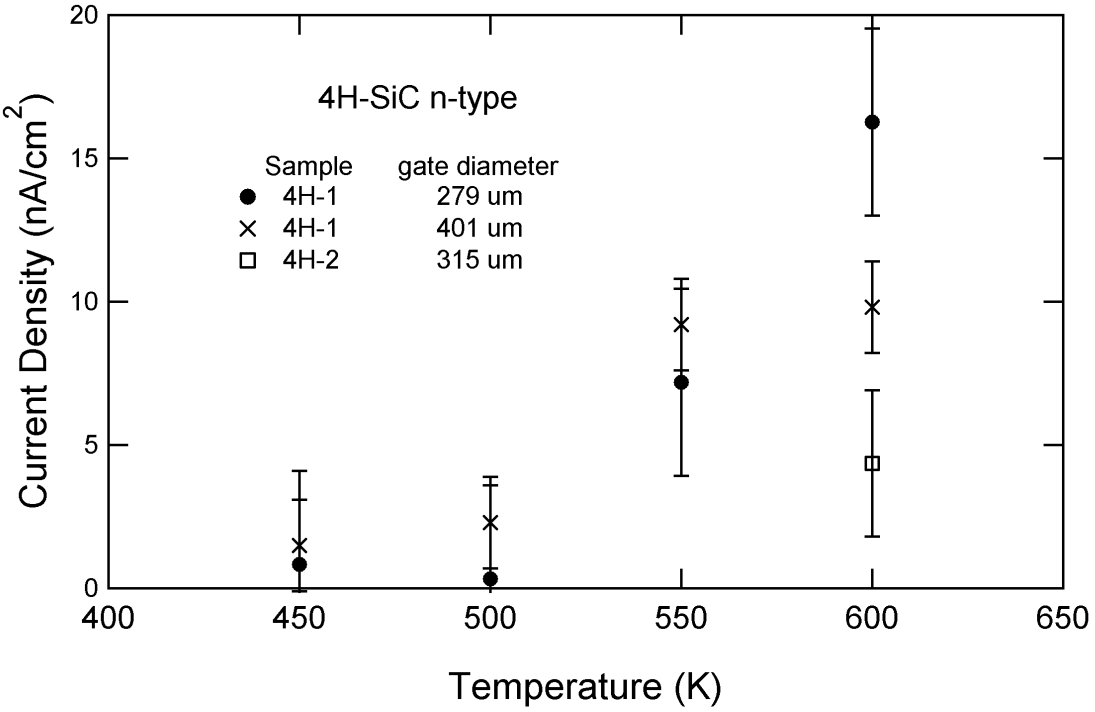

Fig. 4.2.2b. Gate leakage current density as a function of temperature for 4H-SiC n-type devices. See Table 3.4 for details of the device geometry. The capacitor is biased at midgap to optimize device reliability at high temperature.

Our results shown in Figs 4.2.2a and 4.2.2b are very encouraging in terms of the reliability of SiC MOS devices at elevated temperatures. For oxide fields below 0.6 MV/cm we obtain current densities <10 nA/cm^2 and <17 nA/cm^2 at 600 K for the 6H and 4H polytypes respectively. The results are independent of gate diameter, which ranged from 220 - 550 μm. Biasing at midgap significantly reduces the field across the gate oxide, which in turn lowers the oxide current, resulting in longer device lifetimes at higher temperature. Note that at high temperature our 4H-SiC results are similar to those obtained for 6H-SiC; power electronics applications currently favor the 4H polytype due to its higher electron mobility.

4.3 UHV surface chemistry of the Pt gate

4.3.1 CO adsorption and temperature calibration

We have investigated the adsorption of carbon monoxide (CO) on the cleaned Pt surface of the UHV sample, in order to verify the condition of the surface, test the TPD system, and check the accuracy of the sample thermometry. Fig. 4.3.1 shows a TPD scan following exposure of the sample to 44 L CO at 180 K. (L = Langmuir; 1 L = 10^{-6} Torr s; an exposure of 1 L is approximately enough to cover the surface with a single monolayer if all the molecules stick; an exposure of 44 L CO is enough to fully saturate the surface, but at this temperature multilayers of CO do not form.)

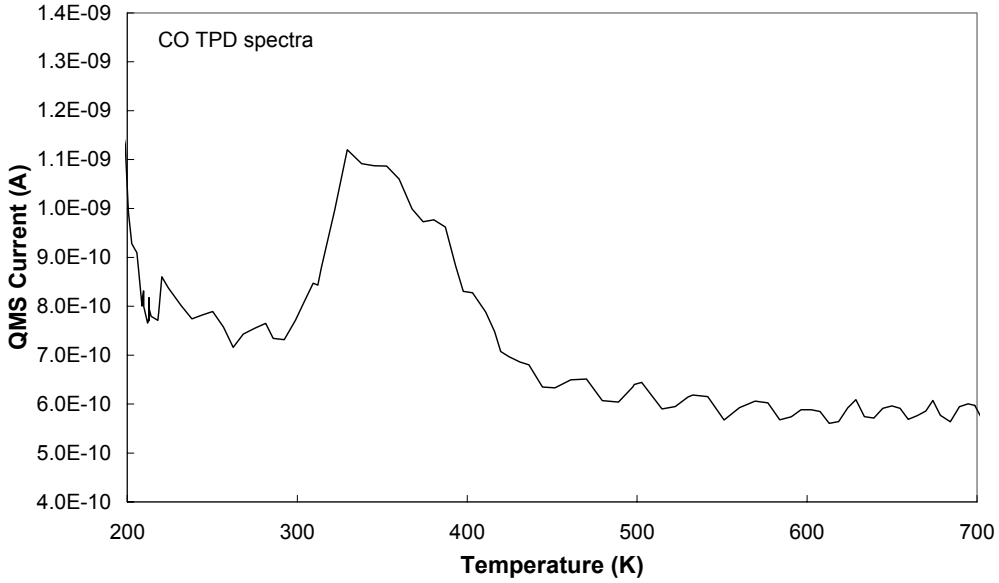

Fig. 4.3.1. TPD spectrum (mass 28) after CO adsorption at 180 K.

This spectrum demonstrates that we have sufficient sensitivity to measure TPD signals from submonolayer gas coverages. The temperature and shape of the desorption peak are in generally good agreement with published results for Pt(111) [Gland 1983, Szabo 1989, Skelton 1999], although the peak temperature we measure is approximately 40 K lower than has generally been reported. This may indicate that our measured temperatures are slightly lower than the true surface temperature. The absence of additional CO desorption peaks at higher temperatures indicates that the surface is almost entirely (111) oriented with only a small density of atomic steps and other defects. This conclusion is consistent with the x-ray diffraction results reported in our previous semi-annual report.

4.3.2 Sulfur contamination studies

We have carried out a series of experiments to investigate sulfur adsorption on the Pt surface and the interactions of adsorbed S with oxygen and hydrogen. To this point we have not succeeded in chemically removing adsorbed S with either gas, but we believe that the problem is largely due to interference from background carbon monoxide and can be overcome by the use of a gas doser.

In Figs. 4.3.2a and 4.3.2b the ordinate represents the intensity ratio of two Auger peaks, one at 152 eV that includes contributions from both Pt and S, and one at 237 eV that is due entirely to Pt. Thus this ratio is indicative of the amount of adsorbed sulfur, with a value near one representing the clean Pt surface. The figure shows the evolution of the sulfur coverage through various surface treatments.

The first two points in Fig. 4.3.2a show the increase in sulfur coverage when the sample is exposed to 1.5×10^{-7} Torr H_2S for 30 min at a sample temperature of 700 K. Clearly sulfur is deposited on the surface under these conditions. Argon sputtering

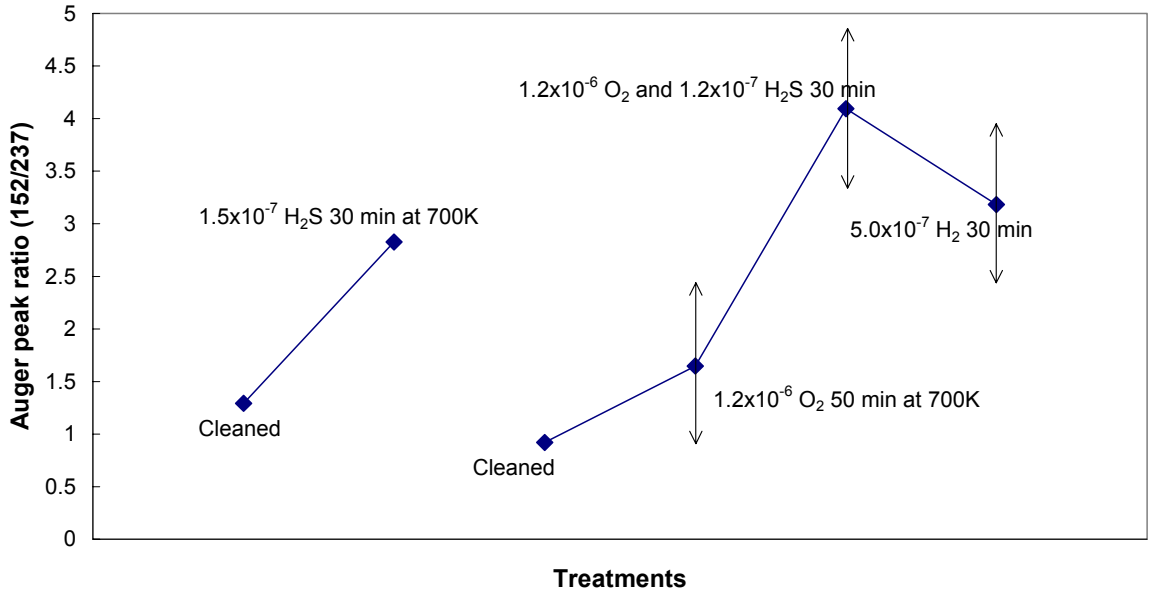

Fig. 4.3.2a. Evolution of the surface coverage of sulfur during various treatments in UHV. An Auger ratio of one represents the clean Pt surface. The double-ended arrows on the last three points are error bars and are due to noise in the spectra when the measurements are made at elevated sample temperatures, with the sample heater turned on. For the first three points the error bars are comparable to the size of the symbol.

returns the sample to its clean state, as shown by the third point. The next point shows that exposure to 1.2×10^{-6} Torr oxygen for 50 min. at 700 K produces no significant increase in the sulfur level; this experiment verifies that there is not a problem with residual sulfur in the gas or in the Pt. H_2S was then admitted to the chamber at a concentration one-tenth that of the oxygen, 1.2×10^{-7} Torr, and the sample was exposed to the O_2/H_2S gas mixture for 30 min. This resulted in a large increase of the sulfur coverage, showing that the oxygen did not prevent the deposition of sulfur. Finally, the sulfur-covered sample was exposed to 5.0×10^{-7} Torr hydrogen for 30 min at 700 K, with negligible reduction in the sulfur level. Thus hydrogen was unable to remove the sulfur from the already-covered Pt surface.

Fig. 4.3.2b shows the results of several attempts to remove adsorbed sulfur from the Pt surface by exposure to oxygen. Previous surface science studies have shown that coadsorbed oxygen and sulfur will react to form SO_2 at temperatures of about 500 K and above, provided the sulfur coverage is no higher than about 0.25 monolayer (ML) [Astegger 1982]. The first two pairs of points show that there was negligible change in the sulfur coverage when the sample was repeatedly cycled between 380 K and 700 K in two different oxygen pressures. The last two groups of points illustrate experiments in which sulfur was first deposited on the surface, the surface was then exposed to oxygen at low temperature, and finally the sample was heated in a TPD experiment. For both high and low sulfur coverages, little change was observed.

During these last two experiments, the QMS was also used to look for the SO_2 desorption that is characteristic of sulfur oxidation, and that was observed by Astegger

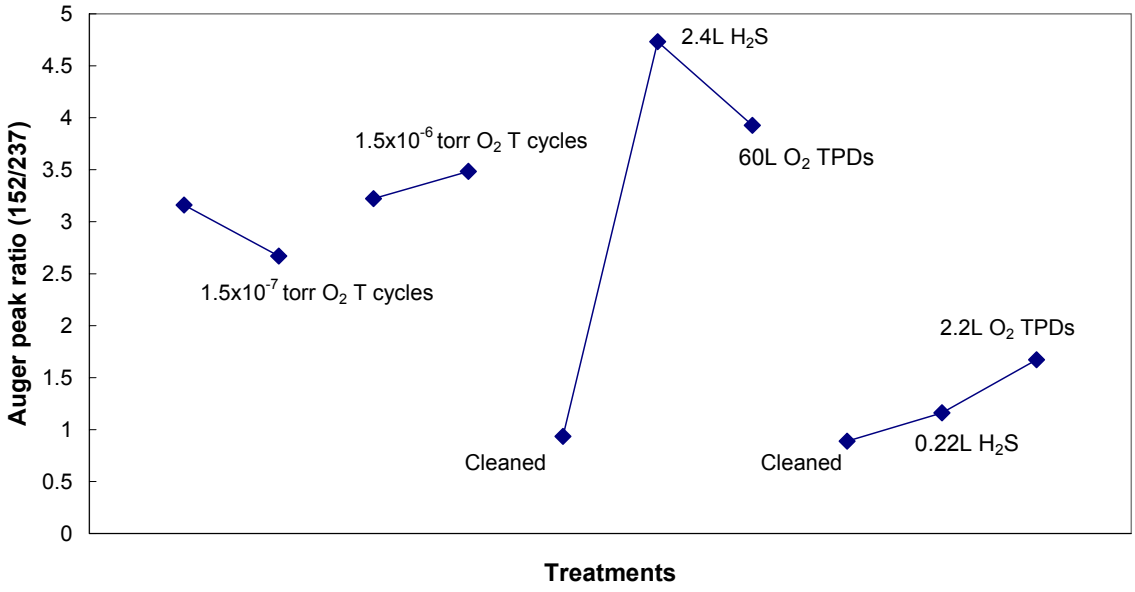

Fig. 4.3.2b. Evolution of the surface coverage of sulfur during various treatments in UHV. An Auger ratio of one represents the clean Pt surface.

and Bechtold near 500 K. Fig. 4.3.2c shows the data, in which no desorption of SO or SO_2 is detectable.

We believe that the absence of any reaction between oxygen and adsorbed sulfur in our experiments is due to interference with background CO in the chamber. It is well known that oxygen exchanges with CO on the walls of stainless steel UHV chambers,

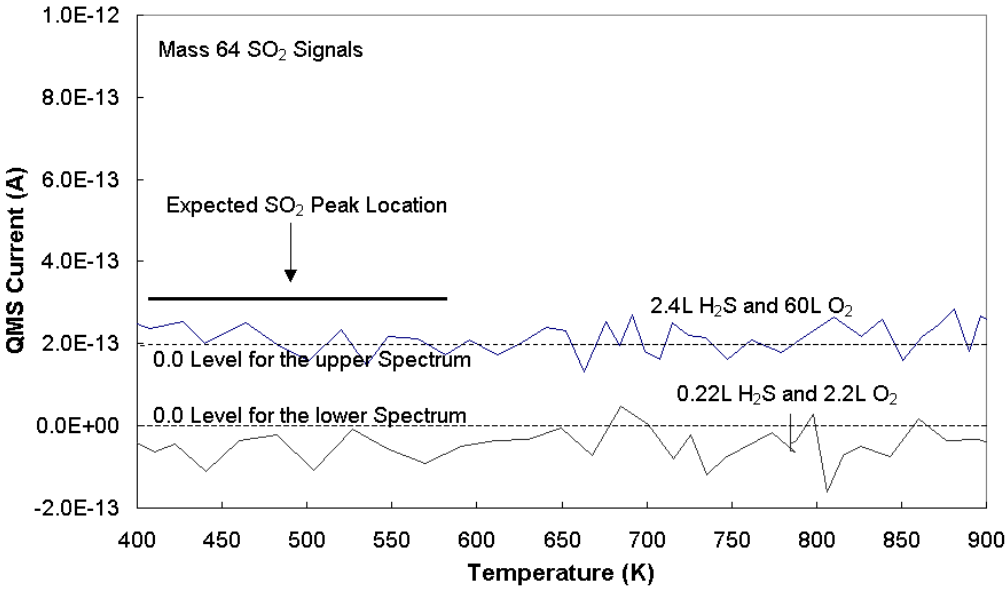

Fig. 4.3.2c. SO_2 TPD traces for two experiments in which a surface with adsorbed sulfur was exposed to oxygen at low temperature and then heated. According to published reports an SO_2 desorption peak is expected between 400 and 600 K [Astegger 1982].

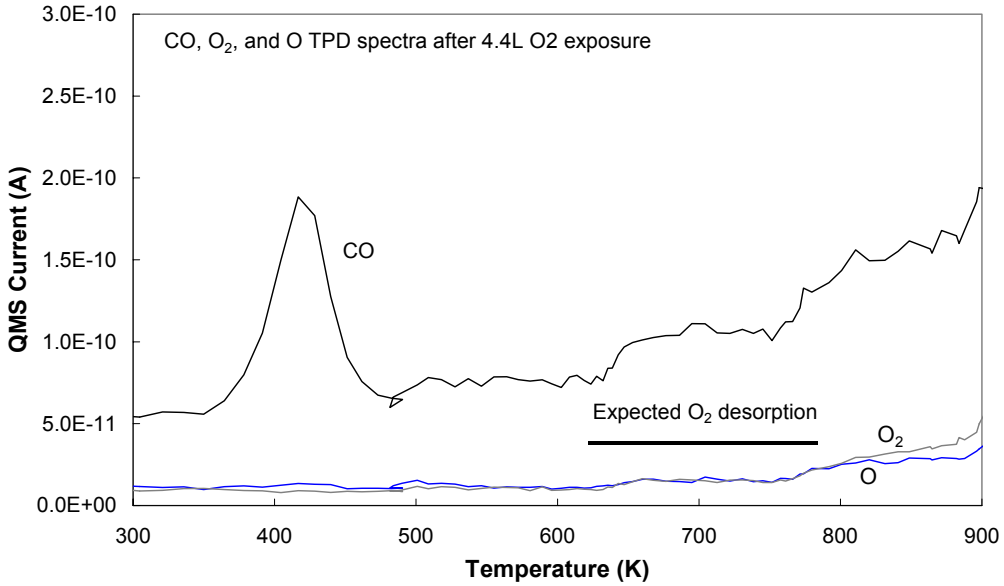

Fig. 4.3.2d . TPD spectra after O_2 exposure onto the clean Pt surface. The large CO desorption, and absence of any oxygen desorption signal, demonstrate that only CO is adsorbed on the surface.

leading to relatively high CO/O_2 ratios in the chamber even when pure O_2 is admitted, and that the high CO level can prevent the adsorption of oxygen on Pt. Fig. 4.3.2d demonstrates that this effect is occurring in our chamber. It shows TPD traces for CO and oxygen following exposure of the sample to *oxygen* at 180 K. Even though only oxygen was admitted to the chamber, only CO is adsorbed on the sample.

The absence of adsorbed oxygen following oxygen exposure was also confirmed by measuring Auger spectra after oxygen exposure and by looking for CO_2 production in TPD following exposure of the surface to both CO and oxygen. All of the results were consistent with only CO being present on the surface.

To avoid this problem, which is specific to the UHV environment and would not be expected in applications, we will install a gas dosing system in which the gas is admitted directly onto the surface, rather than simply filling the chamber with a uniform pressure. Such devices are well known in surface science and are highly effective at avoiding background interference problems [Kuhl 1995]. They also allow the same effective gas flux at the surface to be obtained with a greatly reduced load on the vacuum pumps, which will permit us to maintain a cleaner vacuum and improve experimental efficiency. We will then resume the examination of sulfur removal from the surface by both oxidation to SO_2 and reduction to H_2S.

5. CONCLUSION

We have investigated the reliability of n-type SiC field-effect devices on 4H and 6H substrates in terms of the high temperature stability of the dielectric layer and the gate metallization. The Pt sensing gate was stable under repeated cycling up to 1100 K. The optimum sensor bias point in terms of device-to-device repeatability and high temperature stability of the gate oxide is near midgap. The gate leakage current density at 600 K was measured to be <10 nA/cm^2 and <17 nA/cm^2 for devices fabricated on the 6H and 4H polytypes respectively. The leakage measurements were independent of specific device fabrication procedures such as gate oxidation or metallization technique as well as gate size, which ranged from 220 - 550 μm in diameter. Our results are promising for the development of robust SiC MOS devices for high temperature applications.

Our new apparatus for fast sensor measurements allows us to characterize different sensors both for their fast response in the first milliseconds as well as possible slow contributions after many minutes. With it, we can optimize the sensor structure to increase the fast part and reduce the slow contributions of the sensor response.

We have developed and demonstrated capabilities for *in situ* ultrahigh vacuum surface chemistry measurements on the Pt gate, including heating, cooling, cleaning, Auger electron spectroscopy and temperature-programmed desorption. Initial experiments show that sulfur contamination from ambient hydrogen sulfide gas is a possible problem, and experiments on sulfur removal with oxygen or hydrogen are in progress.

ACKNOWLEDGEMENTS

We thank Dr. Hui Hu and Prof. Manooch Koochesfahani for a fruitful collaboration in characterizing our novel measurement set-up for fast sensors in their laboratory. We also thank Dr. Reza Loloee for the sputter deposition of the Pt films, Mr. Nate Verhanovitz for programming our measurement software, and the staff of the MSU machine shop for fabricating the sputtering masks.

REFERENCES

[Afanas'ev 1996] V. V. Afanas'ev, M. Bassler, G. Pensl, and M. J. Schulz, "Band offsets and electronic structure of SiC/SiO2 interfaces", J. Appl. Phys. 79, 3108 - 3114 (1996).

[Astegger 1982] St. Astegger and E. Bechtold, "Adsorption of sulfur dioxide and the interaction of coadsorbed oxygen and sulfur on Pt(111)," Surf. Sci. **122**, 491 (1982).

[Beadle 1985] W. E. Beadle, J. C. Tsai and R. D. Plummer, *Quick Reference Manual for Si Integrated Circuit Technology,* 6-34, Wiley, New York (1985).

[Cree] Cree Research Inc., Durham, NC 27703, USA.

[Filippov 1999] V. I. Filippov, A. A. Vasilev, A. A. Terentev, W. Moritz and U. Roth, "Sensor Based on a Pt/LaF3/SiO_2/SiC Structure for the detection of chlorofluorocarbons", Tech. Phys. **44**, 1334-1339 (1999).

[Das 2004] M. K. Das "Recent advances in (0001) 4H-SiC MOS device technology", Mat. Sci. Forum **457 - 460**, 1275 - 1280 (2004).

[Dimitrijev 2003] S. Dimitrijev and P. Jamet, "Advances in SiC power MOSFET technology", Micro. Rel. **43**, 225 -233 (2003).

[Ghosh 2002] R. N. Ghosh, P. Tobias, S. Ejakov and B. Golding, "Interface States in High Temperature SiC Gas Sensing", Proc. IEEE Sensors 2002, **2**, 1120-1125, paper 6-4 (2002).

[Gland 1983] J.L. Gland and E.B. Kollin, "Carbon monoxide oxidation on the Pt(111) surface: Temperature programmed reaction of coadsorbed atomic oxygen and carbon monoxide," J. Chem. Phys. **78**, 963 (1983).

[Hunter 2000] G. W. Hunter, P. G. Neudeck, M. Gray, D. Androjna, L.-Y. Chien, R. W. Hoffman, Jr., C. C. Liu and Q. H. Wu, "SiC-based Gas Sensor Development', Mater. Sci. Forum **338-342**, 1439-1422 (2000).

[Katsuta 1979] H. Katsuta ad R. B. McLellan, J. Phys. Chem. Solids, "Diffusivity, Permeability and Solubility of Hydrogen in Platinum", **40**, 697-699, (1979).

[Keithley] "Model 90 - I-V Characterization System" and "Model 82 - WIN Simultaneous C-V System", Keithley Instruments, Inc., Cleveland OH.

[Kim 2001] C. K. Kim, J. H. Lee, S. M. Choi, I. H. Noh, H. R. Kim, N. I. Cho, C. Hong and G. E. Jang, "Pd and Pt SiC Schottky Diodes for Detection of H_2 and CH_4 at High Temperature", Sensor. Actuat. B-Chem. **77**, 455-462 (2001).

[Kuhl 1995] D.E. Kuhl and R.G. Tobin, "On the design of capillary and effusive gas dosers for surface science," Rev. Sci. Instrum. **66**, 3016 (1995).

[Lipkin 1996] L. A. Lipkin and J. W. Palmour, "Improved Oxidation Procedures for Reduced SiO_2/SiC Defects", J. Electron. Mater., **25**, 909-915, (1996).

[Lozano 1992] Lozano, Xip, and Hanson, Experiments in Fluids, **13**, p. 369, (1992).

[Lundstrom 1976] I. Lundström and T. DiStefano, "Influence of Hydrogen on Pt-SiO_2-Si Structures", Sol. St. Comm. **19**, 871-875 (1976).

[Maranowski 1998] M. M. Maranowski and J. A. Cooper, Jr., "Time-Dependent-Dielectric-Breakdown Measurements of Thermal Oxides on N-Type 6H-SiC", IEEE Trans. Electron. Devices 46, 520-524 (1998).

[Nakagomi 2001] S. Nakagomi, Y. Shindo, and Y. Kokubun, "Stability of electrical properties of high-temperature operated H-2 sensor based on Pt-I-SiC diode" Phys. Stat. Solidi A **185**, 33-38 (2001).

[Piconics] Piconics Inc., Tyngsboro MA 01879.

[Samman 2000] A. Samman, S. Gebremariam S, L. Rimai L, X. Zhang, J. Hangas and G. W. Auner, "Silicon-carbide MOS Capacitors with Laser-ablated Pt Gate as Combustible Gas Sensors", Sensor. Actuat. B-Chem. **63**, 91-102 (2000).

[Serina 2001] F. Serina, K. Y. S. Ng, C. Huang, G. W. Auner, L. Rimai and R. Naik, "Pd/AlN/SiC Thin-film Devices for Selective Hydrogen Sensing", Appl. Phys. Lett. **79**, 3350-3352 (2001).

[Senzaki 2004] J. Senzaki, M. Goto, K. Kojima, K. Yamabe and K. Fukuda, "A long-term reliability of thermal oxides grown on n-type 4H-SiC wafer", Mat. Sci. Forum **457 - 460**, 1269 - 1274 (2004).

[Skelton 1999] D.C. Skelton, R.G. Tobin, D.K. Lambert, C.L. DiMaggio, and G.B. Fisher, Oxidation of CO on Gold-Covered Pt(335), J. Phys. Chem. B 103, 964-971 (1999).

[Spetz 2001] A. Lloyd Spetz, L. Unéus, H. Svennningstorp, P. Tobias, L. G. Ekedahl, O. Larsson, A. Göras, S. Savage, C. Harris, P. Mårtensson, R. Wigren, P. Salomonsson, B. Häggendahl, P. Ljung, M. Mattsson and I. Lundström, "SiC Based Field Effect Gas Sensors for Industrial Applications", Phys. Stat. Solidi A **185**, 15-25, (2001).

[Szabo 1989] A. Szabó, M. Kiskinova and J.T. Yates, Jr., "Carbon monoxide-oxygen interaction on the Pt(111) surface: An electron stimulated desorption ion angular distribution (ESDIAD) study," J. Chem. Phys. **90**, 4604 (1989).

[Tobias 2003A] P. Tobias, B. Golding and R. N. Ghosh, "Interface states in high-temperature gas sensors based on silicon carbide", invited issue of IEEE Sensors Jour. **2**, 543-547, (2003).

[Tobias 2003B] P. Tobias, G. Golding and R. N. Ghosh, "Sensing Mechanisms of high temperature silicon carbide field-effect devices", Transducer 2003, paper 2E4.P (2003).

[Wang 2000] X. W. Wang, Z. J. Luo and T. P. Ma, "High-temperature characteristics of high-quality SiC MIS capacitors with O/N/O gate dielectric", IEEE Trans. Electron Devices **47,** 458 - 463 (2000).

BIBLIOGRAPHY

None

LIST OF ACRONYMS AND ABBREVIATIONS

SiC – silicon carbide

SiO_2 – silicon dioxide

MISiC – metal insulator silicon carbide (device)

Quasi-static – calculated C-V from the charge flowing onto a sensor at each voltage step

TPD – temperater programmed desorption

QMS – quadrupole mass spectrometer

AES – Auger electron spectroscopy

UHV – ultra high vacuum